Space Potential Fluctuation in an Anode-layer Hall Thruster

IEPC-2005-124

Presented at the 29th International Electric Propulsion Conference, Princeton University,
October 31 – November 4, 2005

Shigeru Yokota*, Kimiya Komurasaki†, and Yoshihiro Arakawa‡
The University of Tokyo, Department of Aeronautics and Astronautics,
Hongo 7-3-1, Bunkyo, Tokyo 113-8656, JAPAN

Abstract: The electrical sheath structure inside a hollow anode and plasma dynamics in a discharge channel were numerically computed using a fully kinetic2D3V Particle-in-Cell (PIC) / Direct Simulation Monte Carlo (DSMC) code. By treating both electrons and ions as particles, temporal and spatial variations of the non-neutral plasma structure near the anode surface were analyzed. As a result, breathing mode ionization oscillation observed in an anode-layer thruster was well reproduced. The potential drop over the anode surface was fluctuated with plasma density fluctuation. Resulting variation of substantial anode area was found enhancing the oscillation.

Nomenclature

B	=	magnetic flux density
D	=	anode hollow width
e	=	electric charge
E	=	electric field strength
I_d	=	discharge current
m	=	particle mass
n	=	number density
t	=	time
V_d	=	discharge voltage
x	=	position
Z	=	distance between anode tip and channel exit
ε_0	=	free space permeability
ϕ	=	space potential
ν	=	collision frequency
r, z, θ	=	cylindrical coordinate

Subscripts

0	=	anode exit
e	=	electron
i	=	ion
n	=	neutral

* Graduated Student, The University of Tokyo , yokota@al.t.u-tokyo.ac.jp
† Associate Professor, The University of Tokyo, komurasaki@al.t.u-tokyo.ac.jp
‡ Professor, The University of Tokyo, arakawa@al.t.u-tokyo.ac.jp

I. Introduction

Discharge instability in anode layer hall thrusters would be one of the serious problems to be overcome. A hollow anode is commonly used to stabilize the discharge for these thrusters.[1-3)] However, the mechanism of discharge stabilization using a hollow anode has not been clarified yet and optimization of anode design has not been done.

The goal of our study is to model the anode sheath, which has a great effect on the stable discharge of anode layer hall thrusters, and find out a scaling law for the anode design.

In the computational study, the structure of electrical sheath inside a hollow anode was numerically simulated using fully kinetic 2D3V Particle-in-Cell (PIC) and Direct Simulation Monte Carlo (DSMC) methodologies.[4-9)] The results are compared with the measurement using a 1-kW class anode layer hall thruster.

II. Discharge Current Oscillation

A 1kW-class anode layer hall thruster with a hollow anode has been designed and fabricated as shown in Fig. 1. It has two guard rings made of stainless steel. They are kept at the cathode potential. The inner and outer diameters of a discharge chamber are 48mm and 62mm, respectively. Magnetic flux density is variable by changing the current of a solenoid coil set at the center of the thruster. Detailed description is available in Refs. [3,4)].

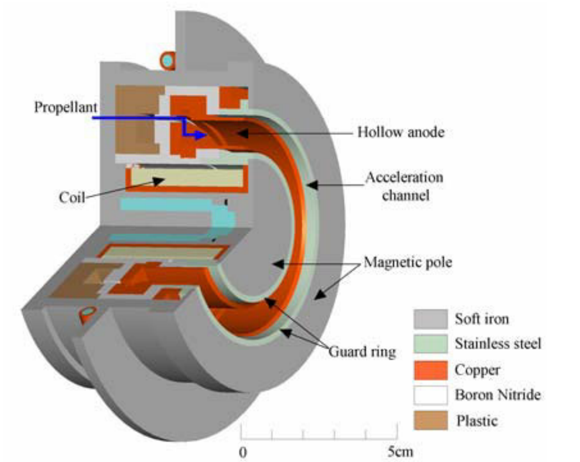

Figure 1. The University of Tokyo Anode Layer Hall Thruster.

Figure 2. Photograph of the Hollow Anode.

A photograph of the Hollow Anode is shown in Fig. 2. It has an annular hollow anode made of cupper. We define Z as the distance between the thruster exit and the tip of anode, and D as the width of propellant channel. Z and D are varied (Z=1~4mm, D=1~3mm) in this study. Xenon is used as a propellant, and the mass flow rate is set at $1.0\mathrm{A_{eq}}$=1.37mg/s. Discharge voltage is set at 400V.

Figure 3 shows measured amplitude of discharge current oscillation and the time-averaged discharge current $\overline{I_d}$. Here, the amplitude of discharge current oscillation is defined as,

$$\Delta = \sqrt{\int_0^\tau (I_\mathrm{d}/\overline{I_\mathrm{d}} - 1)^2 \mathrm{d}t \Big/ \tau} \ . \tag{1}$$

Oscillation amplitude was sensitive to magnetic flux density B. Although the oscillation is small at B<0.014T, the thrust efficiency is poor in this range of B because of large electron backflow current. Therefore, the desirable operation condition is limited in a quite narrow range of B.

Measured oscillation amplitude is plotted for various anode geometries in Fig. 4. There is a common trend that oscillation becomes unstable with the increase in B as seen in Fig. 3. The threshold of B is about 0.011-0.015[T].

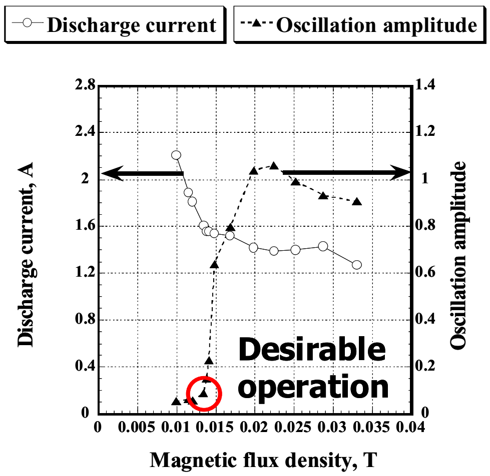

Figure 3. Oscillation characteristics.[4] D=3mm, Z=1mm.

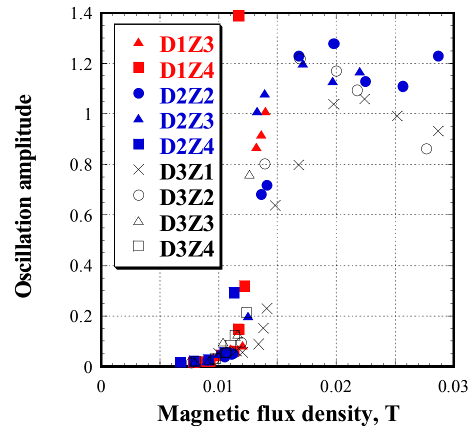

Figure 4. Relation between oscillation amplitude and B. Z=1–4mm, D=1–3mm, Vd=400V. [4]

III. Computation Method

It is very difficult to measure the distributions of electric potential and plasma density inside a hollow anode because plasma density is expected very small and the plasma is electrically non-neutral. Therefore, structure of electrical sheath inside the hollow anode and plasma dynamics in the discharge channel were numerically computed using fully kinetic 2D3V Particle-in-Cell (PIC) and Direct Simulation Monte Carlo (DSMC) methodologies. By treating both electrons and ions as a particle, non-neutral plasma structure in the sheath region near the anode surface can be analyzed. Figure 5 shows the flow chart of calculation.

10^6-10^9 of real particles are treated as one macro particle and all of macro particles are treated kinetically. Electric and magnetic forces are implemented via the PIC method and collisions are via the DSMC method. The cylindrical coordinate system (r, z, θ) was used as shown in Fig. 6. Particle's position is expressed in two-dimensional space r and z, while its velocity is expressed in three-dimensional space. That is, particles move in all directions, but the azimuthal coordinate is always discarded.

An orthogonal calculation grid is set, with the axial length of the cell getting smaller toward the discharge channel in order to observe the sharp fall of electron density in the vicinity of anode exit. The minimum cell length is in the same order of the Debye length.

Figure 7 shows the magnetic flux density distribution used in the calculation, that is identical to the actual distribution in the thruster. [4] B_0 is variable.

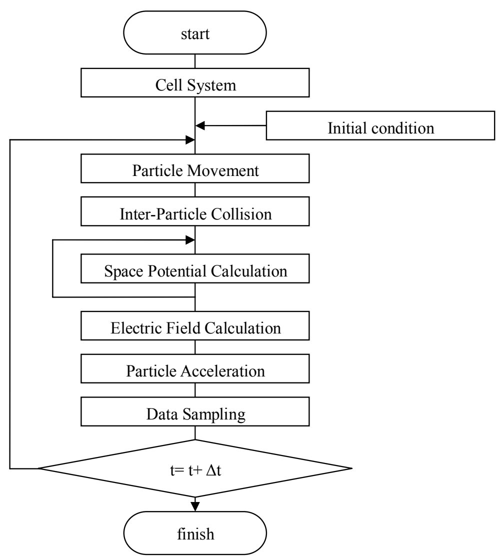

Figure 5. A flow chart of the calculation.

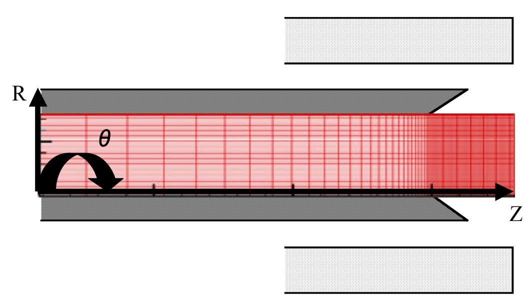

Figure 6. The coordinate and the calculation grid.

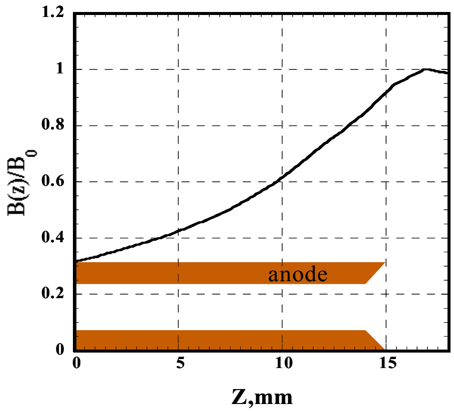

Figure 7. Assumed magnetic flux density distribution.

Table 1. Collisions considered in the Hall Thruster and their typical collision frequency ν.

Collision	Mean Free Time, ps	Relative ν
e^-–Xe Elastic Scattering	2.038	1.00
e^-–Xe Ionization	18.31	0.111
e^-–Xe Excitation	66.83	3.05×10^{-2}
e^-–Xe^+ Coulomb	282.7	7.21×10^{-3}
e^-–e^- Coulomb	15270	1.33×10^{-4}
Xe – Xe Scattering	38300	5.32×10^{-5}

Only singly charged ionization is considered and mass ratio m_e/m_n is decreased from 4×10^{-6} to 1/100, to speed up the calculation. Potential difference between anode and plasma at the thruster exit boundary is set at 250V.

Propellant mass flow rate is set at $1.0A_{eq}$ to simulate the experiment. Electrons are fed from the anode exit with a T_e=10eV half-Maxwellian velocity distribution.

Considerable collisions in the Hall thruster are shown in Table 1. The mean free time and collision frequency ν in the table are typical values when the particles are at their thermal velocity. The three highest frequency collisions are considered in this simulation. The simulation time step (typically 1.22×10^{-11}s) is set based on Larmor frequency, and that is much smaller than e^-–Xe collision mean free time.

In addition, amorous diffusion is considered in this code. The frequency of the Bohm diffusion is

$$\nu_{\mathrm{Bohm}} = \frac{1}{16}\frac{eB}{m_{\mathrm{e}}} . \tag{2}$$

Therefore, total collision frequency is defined as

$$\nu_{\mathrm{total}} = \nu_{\mathrm{elastic}} + \nu_{\mathrm{ionization}} + \nu_{\mathrm{excitation}} + \nu_{\mathrm{Bohm}} . \tag{3}$$

All the particles move according to the dynamic equations. The dynamic equations for electrons are expressed as,

$$m_{\mathrm{e}}\ddot{z} = -e(E_{\mathrm{z}} - r\dot{\theta}B_{\mathrm{r}}) . \tag{4}$$

$$m_{\mathrm{e}}\ddot{r} = -eE_{\mathrm{r}} + m_{\mathrm{e}}r\dot{\theta}^2 . \tag{5}$$

$$m_{\mathrm{e}}r\ddot{\theta} = -e\dot{z}B_{\mathrm{r}} - m_{\mathrm{e}}\dot{r}\dot{\theta} . \tag{6}$$

and for ions,

$$m_{\mathrm{i}}\ddot{z} = eE_{\mathrm{z}} . \tag{7}$$

$$m_{\mathrm{i}}\ddot{r} = eE_{\mathrm{r}} . \tag{8}$$

Space potential ϕ is calculated using the Poisson's equation as,

$$\frac{\partial^2\phi}{\partial z^2} + \frac{1}{r}\frac{\partial}{\partial r}\left(r\frac{\partial\phi}{\partial r}\right) = -\frac{e}{\varepsilon_0}(n_{\mathrm{i}} - n_{\mathrm{e}}) . \tag{9}$$

IV. Code Validation

A. The collision part

The collision section is the most important part of this code and the PIC-DSMC code is compared with the deterministic solution. For easy comparison, the original DSMC code is modified to calculate in one cell. In this code, particles are confined in a certain cell and reflect on the cell boundary. The other parts are same as the original DSMC code.

The equation to solve the collision part deterministically is

$$\frac{dN_n}{dt} = -\frac{N_n N_e \langle \sigma v_e \rangle}{V}. \tag{10}$$

The neutral number which is decay is generated electron number and the sum of these two particles number is constant.

$$N_n + N_e = \text{const.} \tag{11}$$

$<\sigma v_e>$ is a function of electron energy and the equation of the total electron energy conservation is

$$\frac{dE_\mathrm{e}}{dt} = -\dot{N}_\mathrm{ion} E_\mathrm{ion} - \dot{N}_\mathrm{ex} E_\mathrm{ex} \tag{12}$$

where, $\dot{N}_{ion}$ is ionization rate, $\dot{N}_{ex}$ is excitation collision number, E_ion is ionization energy and E_ex is energy loss of excitation collision. The result is shown in Fig.8.

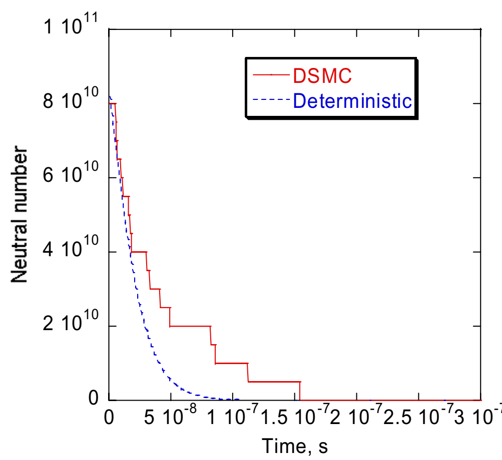

Figure 8. Neutral number history in a cell.
A comparison of the DSMC code solution with the deterministic solution

The characteristic time is defined as a time which neutral number decreases to 1/e. The deterministic solution indicates the characteristic time is about 2.5×10^{-8} s and DSMC solution indicates that is about 3.4×10^{-8} s. This slight difference is caused by small energy electron. In DSMC code, secondary electron, which is generated by ionization, has often too small energy to occur ionization. On the other hand, in deterministic solution, electron energy is averaged in each time step.

Figure 9 shows electron energy distributions at 0 s, 5.0×10^{-9} s, and 1.0×10^{-8} s. At t=0 s, electron energy distribution is Boltzmann distribution. As time increases, small energy electron number increases by ionization and excitation collision and electron energy comes off from Boltzmann distribution. This energy distribution difference makes ionization rate small. As a result, the characteristic time of DSMC code is longer than that of deterministic one.

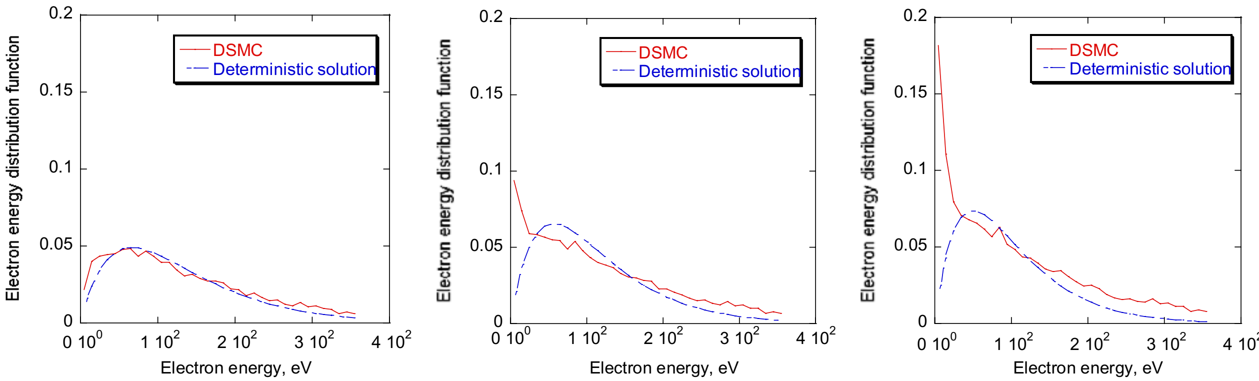

(a) t**=0 s** **(b)** t**=5.0×10^{-9} s** **(c)** t**=1.0×10^{-8}**

Figure 9. Neutral number history in a cell.

B. An error margin by macro-particle

The probabilistic solution is stepwise because one neutral macro-particle is a cluster of real neutrals. Figure 10 shows neutral number history in two cases; in one case, 16 macro particles are in a cell, in the other case, 8331 macro particles are in a cell, initially. For finer resolution, number of neutrals included in a macro particle should be minimized.

In order to find out an adequate macro particle number in a cell, the characteristic time is assumed to be an index. Figure 11 shows the characteristic time in the each macro particle number case. This indicates the characteristic time is about 4.1×10^{-8} s and more than 200 macro particles are necessary in a cell for accurate result.

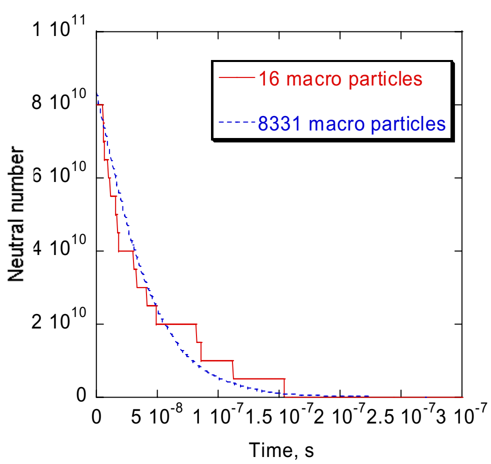

Figure 10. Neutral number history in a cell. *One is a case a macro particle contains 5.0×10^{9} real neutrals. The other is 1.0×10^{7}.*

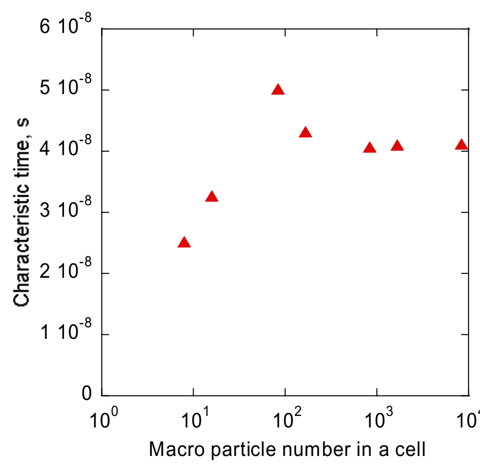

Figure 11. The variations in characteristic time

C. Comparison of DSMC results with experimental results

Finally, calculated results are tested with experimental results.

Figure 12 shows the calculated discharge current histories. In the case of B_0=20mT, strong discharge oscillation was observed. This is ionization oscillation. Oscillation frequency(～50kHz) and the wave shape are very close to the measured one. Averaged discharge current is 0.8A. In this region, the main electron backflow mechanism has transited from classical diffusion to Bohm diffusion in the experiment.

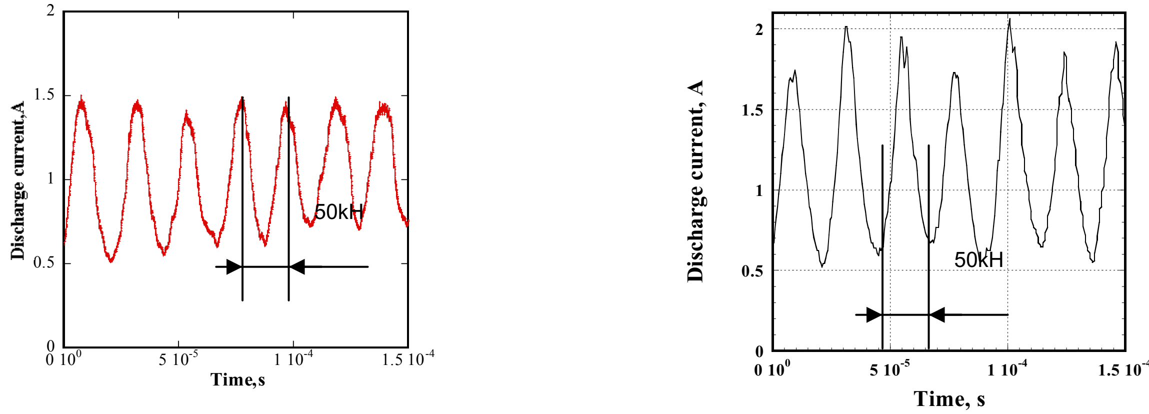

(a) Computed result **(b) Experimental result**

Figure 12. Discharge current history.

V. Results

Figure 13 shows the computed average discharge current and it's oscillation amplitude. The amplitude was high at $B_0 \geqq 0.015$T. This trend agrees well with the measured one as seen in Figs. 3 and 4.

Calculated two-dimensional distributions of electron number density are shown in Fig. 10. In the case of $B_0 \leqq 0.014$T (Fig.14 (a) and (b)) the distributions are stable. For B_0=0.010T, magnetic confinement against the electron backflow is not enough and large electron current flows in the discharge channel. In the case of B_0=0.014T, electron is trapped by the magnetic field, and density peaks in the middle of discharge channel. Plasma has penetrated into the anode cavity resulting in large substantial anode surface area that contacts the plasma. Then, electrons would be able to reach the anode smoothly without a large sheath drop. The ionization reaction inside the hollow anode contributes to this profile. The fraction of propellant gas that is ionized in the hollow anode is about 30%.

In the case of $B_0 \geqq 0.015$T (Fig.14 (c) and (d)) the discharge is oscillating. The island of high-density electrons seen inside

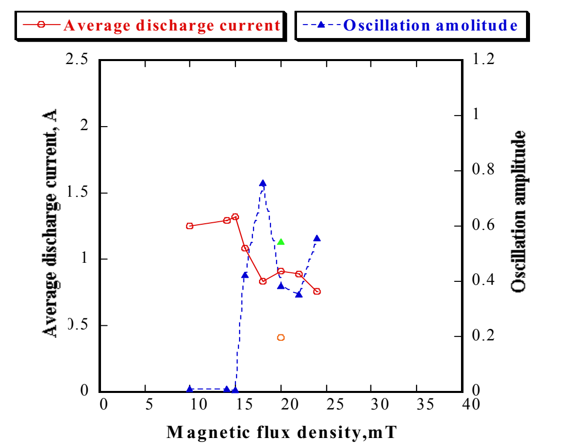

Figure 13. Computed discharge current oscillation amplitude

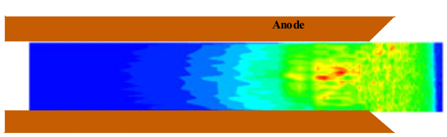

(a)B_0=0.010T

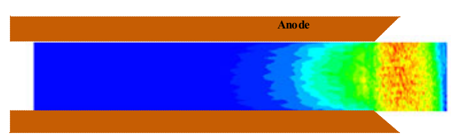

(b)B_0=0.014T

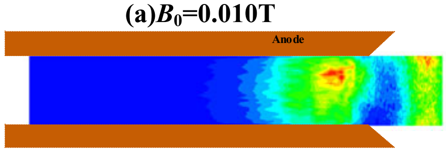

(c)B_0=0.015T

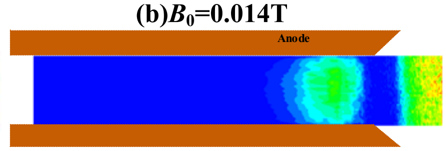

(d) B_0=0.020T

Figure 14. Computed electron number density distributions.

Contour max 2.0×10^{18}m^{-3}, min 0.2×10^{18}m^{-3}. (a) and (b) are steady solutions. (c) and (d) are snapshots of oscillating profiles.

the hollow anode is moving back and forth in the z-direction. Although the gas is ionized inside the hollow anode, the density distribution is discontinuous and ionization instability has seen observed.

Figure 15 shows electron current density distribution on the anode surface. The anode length effective for electron current is about 10mm for D=3mm. Figure 16 shows the computed plasma potential distributions. In the case of $B_0 \leqq 0.014$T, a potential drop appears at the exit of discharge channel. The plasma potential is linearly varied though the anode exit

In the case of $B_0 \geqq 0.015$T, potential starts to decrease at the anode exit. This rapid potential decrease at the anode exit is identical to the one without an anode hollow. The electron density tends to be small due to the rapid acceleration by the electric field resulting in shortage of plasma density on the anode surface.

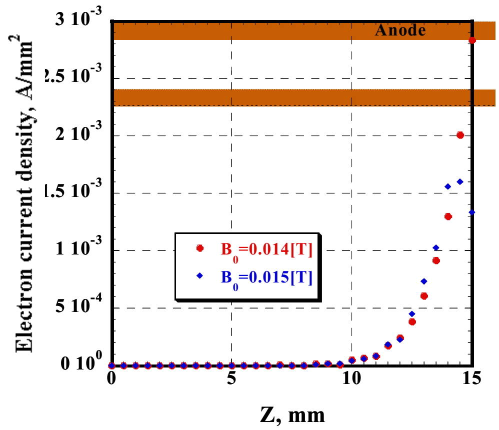

Figure 15. Discharge current distribution on the anode surface.

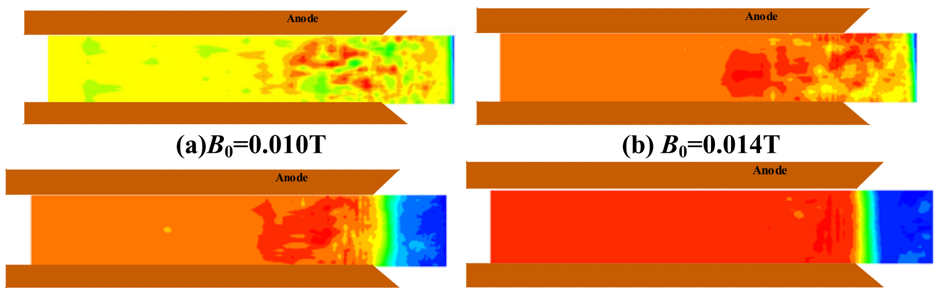

(a)B_0=0.010T **(b) B_0=0.014T**

(c)B_0=0.015T **(d) B_0=0.020T**

Figure 16. Computed electric potential distributions.

Contour max 250V, min 0V. (a) and (b) are steady solutions. (c) and (d) are snapshots of oscillating profiles.

Figure 17 shows the computed electron temperature distributions. In the case of $B_0 \geqq 0.015$T, high temperature region is limited in a thin layer located at the exit of anode. This is due to the strong electric field as seen in Fig. 16. This rapid increase in temperature contributes to the high ionization rate inside the hollow anode, and brings the ionization oscillation inside the hollow anode. To suppress the ionization oscillation, linear variation in plasma potential though the anode exit would be necessary.

As seen in Figs. 16-17, ionization and acceleration occurs in a thin layer at the anode exit in the high magnetic flux density cases. This is a typical feature of anode layer type or sheath type thruster.

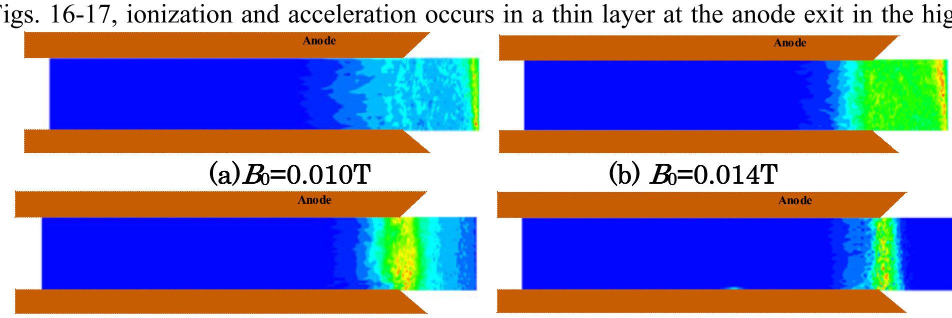

(a)B_0=0.010T (b) B_0=0.014T

(c)B_0=0.015T (d) B_0=0.020T

Figure 17. Computed electron temperature distributions.

Contour max 100eV, min 0eV. (a) and (b) are steady solutions. (c) and (d) are snapshots of oscillating profiles.

The condition in which the layer appears will be a function of operating and geometric parameters of the thruster. Then, optimization of the hollow anode geometry for typical operational condition would be one way to suppress the oscillation. Another way would be to have a discharge independent of the main discharge to assist the ionization in the hollow anode.

VI. Conclusions

The fully kinetic PIC-DSMC code can reproduce both stable and unstable operation modes observed in the experiment.

In the stable operation case, which corresponds to the low magnetic flux density case, the plasma penetrated into the anode cavity. This large substantial anode area would contribute to stable operation.

In the unstable operation case, which corresponds to the high magnetic flux density case, ionization oscillation and space potential fluctuation was observed inside the hollow anode. This would be caused by the non-linear variation of plasma potential at the anode exit.

To suppress the ionization oscillation, linear variation in plasma potential though the anode exit would be necessary.

References

[1]Semenkin A.V., Tverdokhlebov S.O., Garkusha V.I., Kochergin A.V., Chislov G.O., Shumkin B.V., Solodukhin A.V., Zakharenkov L.E., “Operating Envelopes of Thrusters with Anode Layer”, IEPC2001-013, 27th International Electric Propulsion Conference, Pasadena, USA, October 2001.

[2]Semenkin, A., Kochergin, A., Garkusha, V., Chislov, G., Rusakov, A., “RHETT/EPDM Flight Anode Layer Thruster Development”, IEPC-97-106, 25th International Electric Propulsion Conference, Cleveland, USA, August 1997.

[3]Yamamoto, N., Nakagawa, T., Komurasaki, K., Arakawa, Y., “Effect of Discharge Oscillations on Hall Thruster Performance”, ISTS 2002-b-17, 23rd the International Symposium on Space Technology and Science, Shimane, Japan, May 2002.

[4]Yasui, S., Yamamoto, N., Komurasaki, K., Arakawa, Y., “Effect of Sheath Structure on Operating Stability in an Anode Layer Thruster,” Proceedings of Asian Joint Conferences in Propulsion and Power 2004, pp.382-387, Seoul, Korea, March 2004.

[5]Hirakawa, M., “Particle Simulation of Plasma Phenomena in Hall Thrusters”, IEPC-95-164, 24th International Electric Propulsion Conference, Moscow, Russia, September 1995..

[6]Szabo, J. J., “Fully Kinetic Hall Thruster Modeling of a Plasma Thruster”, PhD Thesis, Massachusetts Institute of Technology, 2001.

[7]Szabo, J., Rostler, P., “One and Two Dimensional Modeling of the BHT-1000”, IEPC-02-231, 28th International Electric Propulsion Conference, Toulouse, France, March 2003.

[8]Kumakura, K., Yasui, S., Komurasaki K., Arakawa, Y., “Plasma Modeling of a Hollow Anode for an Anode Layer Type Hall Thruster” IEPC-02-086, 28th International Electric Propulsion Conference, Toulouse, France, March 2003.